

An Investigation of the Mold-Flux Performance for the Casting of Cr12MoV Steel Using a Mold Simulator Technique



LEJUN ZHOU, WANLIN WANG, CHAO XU, and CHEN ZHANG

Mold flux plays important roles in the process of continuous casting. In this article, the performance of mold flux for the casting of Cr12MoV steel was investigated by using a mold simulator. The results showed that the slag film formed in the gap between the initial shell and mold hot surface is thin and discontinuous during the casting process with the Flux BM, due to the absorption of chromic oxide inclusions into the liquid slag, while the slag film formed in the case of the optimized Flux NEW casting process is uniform. The main precipitated crystals in Flux BM slag film are cuspidine ($\text{Ca}_4\text{Si}_2\text{O}_7\text{F}_2$) and Cr_3O_4 , but only $\text{Ca}_4\text{Si}_2\text{O}_7\text{F}_2$ precipitated in the Flux NEW case. Besides, both the responding temperature and heat flux in the case of Flux BM are relatively higher and fluctuate in a larger amplitude. The surface of the shell obtained in the case of the Flux BM experiment is quite uneven, and many severe depressions, cracks, and entrapped slags are observed in the surface due to the lack of lubrication. However, the obtained shell surface in the case of the Flux NEW shows good surface quality due to the addition of B_2O_3 and the adjustment of basicity, which can compensate for the negative effects of the mold-flux properties caused by the absorption of chromic oxide during the casting process.

DOI: 10.1007/s11663-017-0990-0

© The Minerals, Metals & Materials Society and ASM International 2017

I. INTRODUCTION

THE property of mold flux is important in determining the surface quality of the strand during the process of continuous casting, as it can protect the molten steel from oxidation, prevent steel from freezing, and absorb inclusions from molten steel. Besides, it tends to lubricate the shell during the mold oscillation and moderate the heat transfer in the mold when it infiltrates into the mold/shell channel. The properties of mold flux, such as crystallization, heat-transfer ability, viscosity, melting behavior, and surface tension, are used to characterize the performance that the mold flux behaved in the mold. The crystallization of mold flux usually determines the structure and phase (glass, crystalline, and liquid) distribution of slag film in the mold wall/shell gap, which in turn controls the in-mold

heat transfer and lubrication in the continuous casting mold.^[1,2] The heat-transfer capability of mold flux affects the horizontal heat transfer in the mold greatly; an uneven heat transfer and rapid cooling of solidified shell can cause enormous thermal stress on the initial shell, especially for the casting of crack-sensitive high-carbon Cr12MoV alloy steel, which consequently causes cracks and other surface defects on the shell surface.^[3,4] Viscosity is one of the most important properties of mold flux, as it determines the powder consumption and the lubrication of the mold oscillation.^[5] The melting temperature range of the mold flux directly determines the thickness of liquid flux on the top surface of molten steel, which affects the behavior of inclusion absorption, heat insulation, and reoxidation protection.^[6] The surface property of the mold flux usually not only influences the absorption of inclusions, but also affects the size and shape of the slag rim formed in the vicinity of the meniscus, *etc.*^[7,8]

In order to characterize the specific properties of mold flux, many techniques and methods have been developed. For example, differential thermal analysis (DTA),^[9,10] single/double hot thermocouple technology (SHTT/DHTT),^[11–13] and confocal scanning laser microscopy^[14,15] were used to study the crystallization ability of mold flux. The Fourier transform infrared spectrometer,^[16,17] infrared emitter technique,^[18,19] inverse heat-flux simulator,^[20] and several other thermal conductivity measurement methods^[21–23] were

LEJUN ZHOU and CHAO XU are with the School of Metallurgy and Environment, Central South University, Changsha 410083, P.R. China. WANLIN WANG is with the School of Metallurgy and Environment, Central South University, and also with the National Center for International Research of Clean Metallurgy, Central South University. Contact email: wanlin.wang@gmail.com CHEN ZHANG is with the Steelmaking Research Department, Research Institute, Baosteel Group Corporation, Shanghai 201900, P.R. China.

Manuscript submitted November 19, 2015.

Article published online May 22, 2017.

developed to investigate the heat-transfer behavior of mold flux. Besides, the high-temperature viscometer for viscosity measurement,^[24] the high-temperature microscopy technique,^[25] and SHTT^[26] for the melting behavior study, as well as the sessile drop method for the surface/interface property evaluation,^[27] were developed recently.

Although the aforementioned techniques and methods were extensively used to characterize the properties of mold flux, few of them can fully evaluate the overall performance of mold flux in the practical industrial continuous casting process. Although on-site operational experiments regarding the mold-flux properties study were carried out in the real industrial caster,^[28,29] they are inconvenient to operate and would disturb the normal production process.

Badri *et al.*^[30] used a mold simulator to investigate the formation mechanism of oscillation marks. Ko *et al.*^[31] also used a similar method to investigate the behavior of initial solidification of low-carbon steel and mold-flux crystallization. Results from both works suggested that the mold simulator is an efficient tool to simulate the actual situation in continuous casting mold. Therefore, in this article, a mold simulator technique was adopted to investigate the performance of mold fluxes for the casting of Cr12MoV steel based on our previous studies.^[32–34]

II. EXPERIMENTAL METHOD

A. Mold Simulator

The mold simulator applied to this study is an inverse-type mold, which includes seven units: heating furnace, water cooling system, mold oscillator system, shell withdrawal (extractor) system, data acquisition/control system, stage driver unit, and Ar gas protection system, and its schematic figure is shown in Figure 1. The mold with water-cooling grooves is manufactured inside a copper plate, and 16 thermocouples are embedded under the mold hot surface against the liquid steel. The mold is covered with an extractor, leaving one face exposed to the liquid melt. As the liquid steel contacts the mold hot face and forms an initial shell, the extractor withdraws the solidifying shell downward to simulate the continuous casting process; meanwhile, the responding temperatures at the positions that are 3 and 8 mm away from the hot face of the mold, as shown in Figure 1, can be measured by those two column thermocouples with a collection frequency of 60 Hz by using the data acquisition system during the experimental procedures. The details about the mold simulator were described in a previous article.^[32,33]

B. Experimental Procedure

The casting parameters for this study are summarized in Table I, and they are similar to the ones of the actual plant casting process. The raw materials used in these experiments are Cr12MoV steel ([C]: 1.15 to 1.95 wt pct, [Cr]: 9 to 15.5 wt pct), Flux BM, and Flux NEW. Among them, Flux BM is a commercial mold flux, while

flux NEW is an optimized mold flux, and their major chemical compositions are listed in Table II. During the experiments, about 25-kg Cr12MoV steel was melted in an induction furnace with the protection of Ar gas. After the temperature of the melt was adjusted to a target value, 0.3-kg mold-flux powders were added to the surface of the liquid bath so that there would be a layer of molten flux 9-mm thick on top of the liquid steel. Then the copper mold covered with the extractor was pushed into the melt; meanwhile, the mold was kept oscillated. The mold and extractor were lowered to the preset depth into the melt bath, where the meniscus of the liquid steel was located in the mold thermocouple-measuring zone. After the mold and extractor reached the target depth, they were held for 5 seconds to form an initial shell on the water-cooled copper mold to ensure the initial shell was strong enough to prevent tearing during extraction; then the casting was started. The extractor withdrew the solidifying shell downward at a constant speed to simulate the continuous casting process. During casting, the mold itself was moved upward at a certain speed to compensate for the rise of the mold level, so that the meniscus could be kept at the same position with respect to the mold. The liquid mold flux would then infiltrate into the gap between the initial solidified shell and the mold hot face to form the slag film. When the casting was completed for the desired length, the mold and extractor were withdrawn from the furnace and then cooled in air. From the time that the mold started to lower into the bath to the completion of casting, the mold was kept oscillating sinusoidally with the preset frequency and stroke. At last, the solidified shell and slag film adjacent to the copper mold were cut off for further analysis.

The responding temperatures' histories at the preset locations were recorded by Labview software, through an NI data acquisition system. The first column of thermocouples at the distance 8 mm horizontally away from the mold hot surface provided the temperature boundary, while the second column of thermocouples at the distance 3 mm away from the mold hot surface was used to estimate the error between the calculated and measured temperatures. Finally, the responding temperature and heat flux across the mold hot face were obtained by a two-dimensional-inverse heat conduction problem (2D-IHCP); the details about the development and application of 2D-IHCP were described in a previous article.^[35]

C. Slag Film Characterization Method

The slag films formed in the casting process were collected after the experiments. The overall profiles of the slag films were observed through digital microscopy. Then the thickness of the slag film along the centerline was measured by a Vernier caliper. In order to observe the structure of the slag film and the morphology of the precipitated crystalline phase, typical parts of the slag film were sampled and observed through a scanning electron microscope (SEM, JSM-6360LV, Japanese Electronics Company) with an acceleration voltage of 20 kV. Besides, the crystalline phase developed during

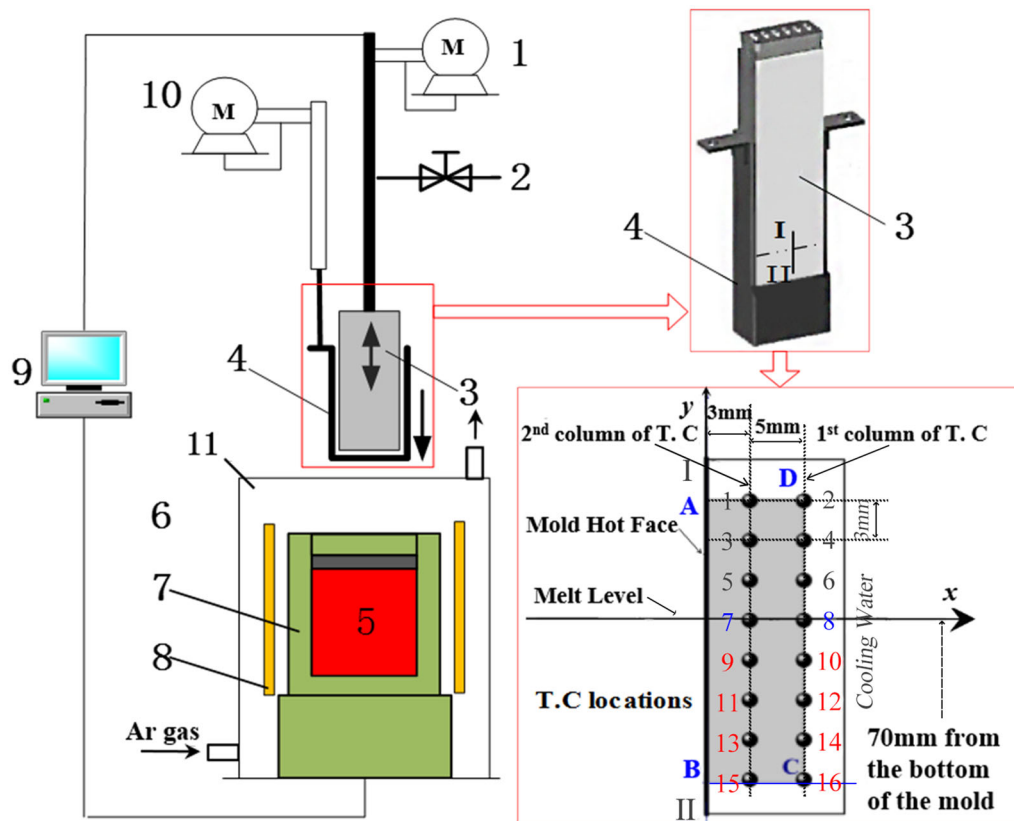


Fig. 1—Schematic figure of the mold simulator: 1—oscillation drive, 2—cooling water, 3—mold, 4—extractor, 5—melt, 6—mold flux, 7—induction furnace, 8—induction coil, 9—data acquisition and control system, 10—extractor drive, and 11—Ar gas protective cover.

Table I. Mold Oscillation Setting and Casting Conditions

Casting Temperature [K (°C)]	Casting Speed (mm/s)	Frequency (Hz)	Stroke (mm)	Water Flow (L/min)
1708 (1435)	12	1.67	±5	7.2

Table II. Major Chemical Compositions of Mold Fluxes Used in This Study (Weight Percent)

Flux	SiO ₂	CaO	Al ₂ O ₃	Na ₂ O + Li ₂ O	F	B ₂ O ₃	MgO	R	Viscosity*	T _{br} **
BM	30 to 35	31.5 to 38	2 to 5	11 to 15	10 to 13	0	1 to 3	0.96	0.12	1302 (1029)
New	31 to 36	30 to 34	2 to 5	11 to 15	10 to 13	3	1 to 3	1.05	0.06	1246 (973)

*Represents the viscosity at 1573 K (1300 °C) (Pa·s).

**Represents the break temperature, K (°C).

the casting experiment was analyzed by an energy dispersive spectrometer (EDX-GENESIS 60S, America EDAX Corporation) and an X-ray diffractometer (RIGAKU-TTR III, Rigaku Corporation). The X-ray diffraction (XRD) data were collected in a range of $2\theta = 10$ to 80 deg with a step size of 10 deg/min.

III. RESULTS AND DISCUSSION

A. Distribution of Slag Film

Figure 2 shows the situation of the gap between the mold and shell after the completion of the casting of Cr12MoV with Flux BM, where the initial solidified

shell was cut off and the slag film was clearly observed either to attach to the copper mold or be entrapped on the surface of the solidified shell. It can be seen that the meniscus of the shell matches the preset line (the top red line) perfectly. The slag film formed in this case is discontinuous and entrapped in the initial shell severely, which indicates the infiltration of the molten slag is not sufficient during the casting process with Flux BM. The reason for that is due to the deterioration of Flux BM properties caused by the absorption of chromic oxide inclusions with a high melting point. Although the experimental process was protected by Ar gas, the oxidation of the alloying element Cr in Cr12MoV steel still occurred, and the precipitated chromic oxide

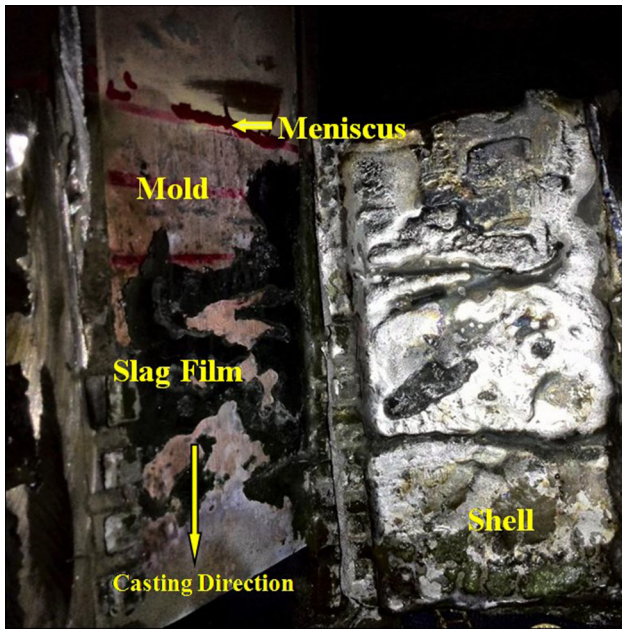


Fig. 2—Shell and slag film formed during the casting experiment with Flux BM.

inclusions floated up and were absorbed into the liquid flux during the experiment. Actually, the oxidation also occurred in the processes of smelting, refining, continuous casting, and transportation during the production of Cr12MoV steel in the plant operation. Previous study^[36] showed that the pickup of Cr_2O_3 in the mold flux would increase its melting point and viscosity greatly, introducing the problem of mold-flux infiltration.

After the experiment, the slag films of Flux BM and Flux NEW were stripped from the copper mold, and they are shown in Figures 3(a) and (b), separately. Due to the mold oscillation and shrinkage of solid mold flux during cooling, the film was broken into pieces, and it is hard to obtain the entire piece of slag film. However, it is clear from Figure 3 that the slag film of Flux NEW is much more uniform than that of Flux BM. The improvement of the infiltration of the optimized Flux NEW mainly results from the addition of 3 wt pct B_2O_3 in the mold flux, which could compensate for the influence caused by the pickup of chromic oxide inclusions. As an effective fluxing agent, the addition of B_2O_3 tends to lower the melting point and viscosity of mold flux,^[18,37] which offers a better infiltration of Flux NEW; thus, a more uniform slag film formed between the shell and mold wall.

In order to further study the slag film structure of Flux BM and Flux NEW, both positions A and B, as shown in Figures 3(a) and (b), were amplified and shown in Figure 4. Circular holes can be found in the slag films, especially close to the mold side for both mold fluxes. They may be caused by the huge temperature gradient between the mold wall and shell.^[38] When the molten slag touched the water-cooled mold wall, it solidified immediately; thus, the holes were formed due to the residual bubbles in the slag during the

liquid-to-solid transformation. Besides, the holes formed in the solidified mold-flux film close to the mold side could not be refilled again due to the low fluidity nature of mold flux in the low-temperature region. The average thickness of both slag films has been estimated and listed in Table III. They are 0.51 and 0.68 mm for Flux BM at positions A and B, while they are 0.62 and 0.85 mm for Flux NEW. Hence, the Flux NEW shows a better infiltration ability in this study.

In order to investigate the morphology and chemical composition of the precipitated crystalline phase in the slag film, part of the Flux BM and Flux NEW at position A in Figure 3 was analyzed by SEM and energy-dispersive spectrometer (EDS). Figure 5 shows the SEM photo and EDS results of Flux BM at position A, among which Figure 5(a) shows the overview of slag film at position A. Figure 5(b) gives the amplified part of the zoom in Figure 5(a), where the crystals appear close to the mold side, and Figure 5(c) shows two typical morphologies of crystalline phases in Flux BM. Figures 5(d) and (e) show the energy spectra of EDS for both crystals, and the specific element content is listed in the table in Figure 5. From Figure 5(b), it can be seen that the number of crystals decreases while the size increases from the mold side to the initial shell side, which is due to the fact that the cooling rate in the mold side is larger than that close to the shell side. Therefore, the driving force for the nucleation at the mold side is larger, leading to more nucleation sites. On the contrary, due to the cooling rate at the shell side being much smaller, the nucleation amount would be less, and the crystal would keep growing in the relative high-temperature zone. The EDS results in Figures 5(d) and (e) suggest that there are two main types of crystals in slag film: the light particles with main components of Si, Ca, O, and F, similar to the composition of cuspidine ($\text{Ca}_4\text{Si}_2\text{O}_7\text{F}_2$), and the block one with the main components of Cr, Mn, and O, which may originate from the chromium oxide and manganese oxide inclusions from the molten steel. Therefore, it is confirmed that the pickup of the chromium and manganese in the spent mold flux is due to the absorption of these oxides into the mold flux during the casting process.

Figure 6 shows the SEM photo and EDS results of Flux NEW at position A in Figure 3(b). Also, Figure 6(a) shows the overview of the Flux NEW slag film at position A, and Figure 6(b) is the amplified zoom in the box part in Figure 6(a). The variation trend of the number and size of crystals in Figure 6(b) is similar to the case in Figure 5(b). However, comparing Figure 5(b) with Figure 6(b), as well as Figures 5(c) and 6(c), it can be found that the crystallization ability of Flux NEW is weaker than that of Flux BM, as more crystals precipitated in Figures 5(b) and (c). Although the basicity of Flux NEW (basicity = 1.05) is slightly higher than that of Flux BM (basicity = 0.96), the addition of B_2O_3 inhibited the general crystallization ability of Flux NEW. Besides, the results of EDS analysis show that the main components of the precipitated crystals in Flux NEW are Si, Ca, O, and F, similar to cuspidine, and the Cr-containing crystal hardly can

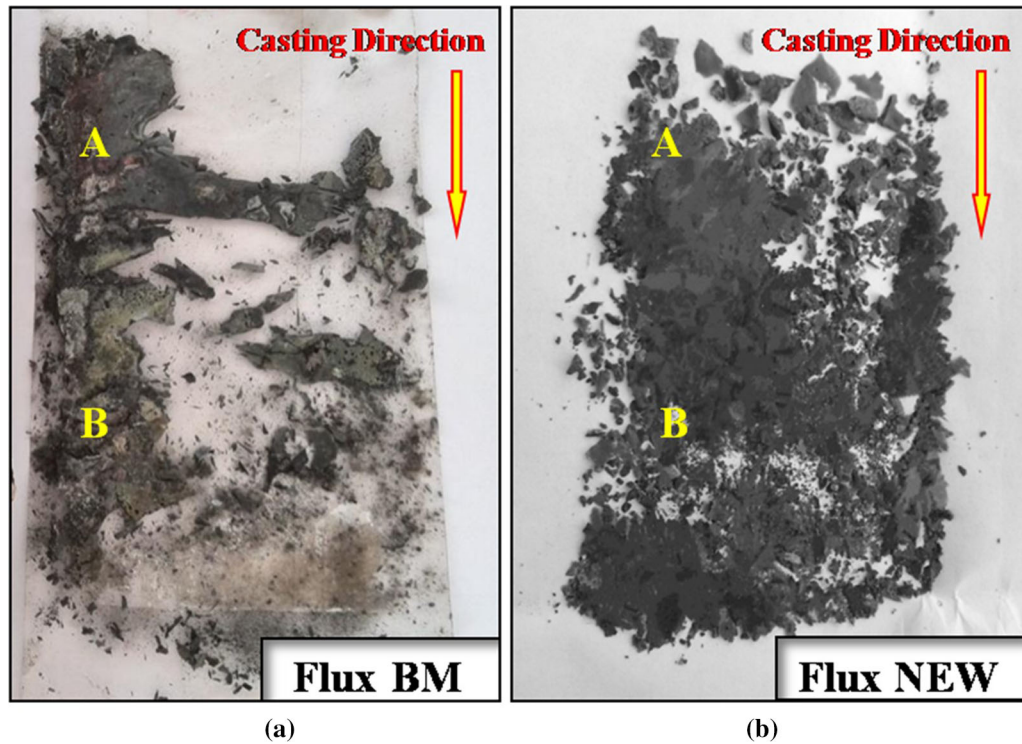


Fig. 3—Distribution of slag films for (a) Flux BM casting and (b) Flux NEW casting.

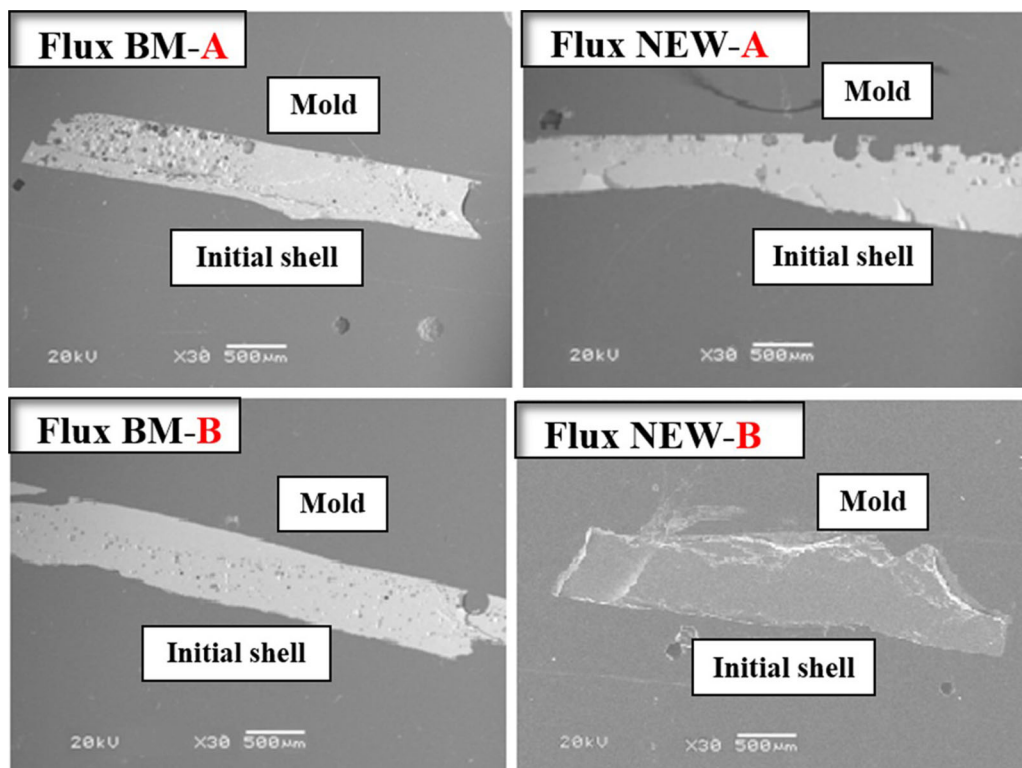


Fig. 4—SEM photos of slag films at positions A and B for Flux BM and Flux NEW.

be found in this slag film, which indicates that B_2O_3 has effectively dissolved the chromium oxides into the high melt matrix.

In order to identify the specific crystalline phase formed in the solid mold-flux film, the collected slag films were further analyzed by XRD, and the XRD

patterns of Flux BM and Flux NEW are shown in Figures 7(a) and (b), respectively. It can be seen from Figure 7(a) that the main characteristic peaks of Flux BM represent the phase of cuspidine ($\text{Ca}_4\text{Si}_2\text{O}_7\text{F}_2$) and Cr_3O_4 , while the main peaks of Flux NEW match well with the characteristics of cuspidine, which is consistent with the EDS results in Figure 6.

B. Responding Temperature and Heat-Flux Analysis

The responding temperatures of the mold hot face were calculated by 2D-IHCP and are shown in Figure 8, where Figure 8(a) is the temperature profile for the case of Flux BM and Figure 8(b) is the temperature profile for the case of Flux NEW. The entire process typically can be divided into four stages.

Table III. Thickness of Flux BM and Flux NEW at Positions A and B

Position	Flux BM (mm)	Flux NEW (mm)
A	0.51	0.62
B	0.68	0.85

Stage I is the mold-dip stage, where the mold temperature increased sharply as the water-cooled mold dipped into the molten bath. Stage II is the holding stage, where the mold was kept in the bath for 5 seconds to ensure the formed initial shell was strong enough to be cast. The responding temperatures were observed to decrease slightly in stage II due to the increase of thermal resistance caused by the initial solidified shell as well as the formation of the shrinkage gap. Stage III is the casting stage, where the responding temperature increased again, as the extractor dragged the initial shell downward and the fresh molten steel touched the mold hot surface again in the vicinity of the meniscus. Stage IV is the drawn-out stage, in which the mold system was drawn out of the melt bath quickly once the casting was completed, so the temperature started to decrease in stage IV. It should be pointed out that the difference of initial dipping time would not influence the comparison of the temperature and heat flux between Flux BM and Flux NEW, as the dipping temperature of both casting experiments was consistent.

Although the casting parameters, experimental process, and general temperature evolution trend are similar, there are still some differences that occur in the responding temperature histories when different

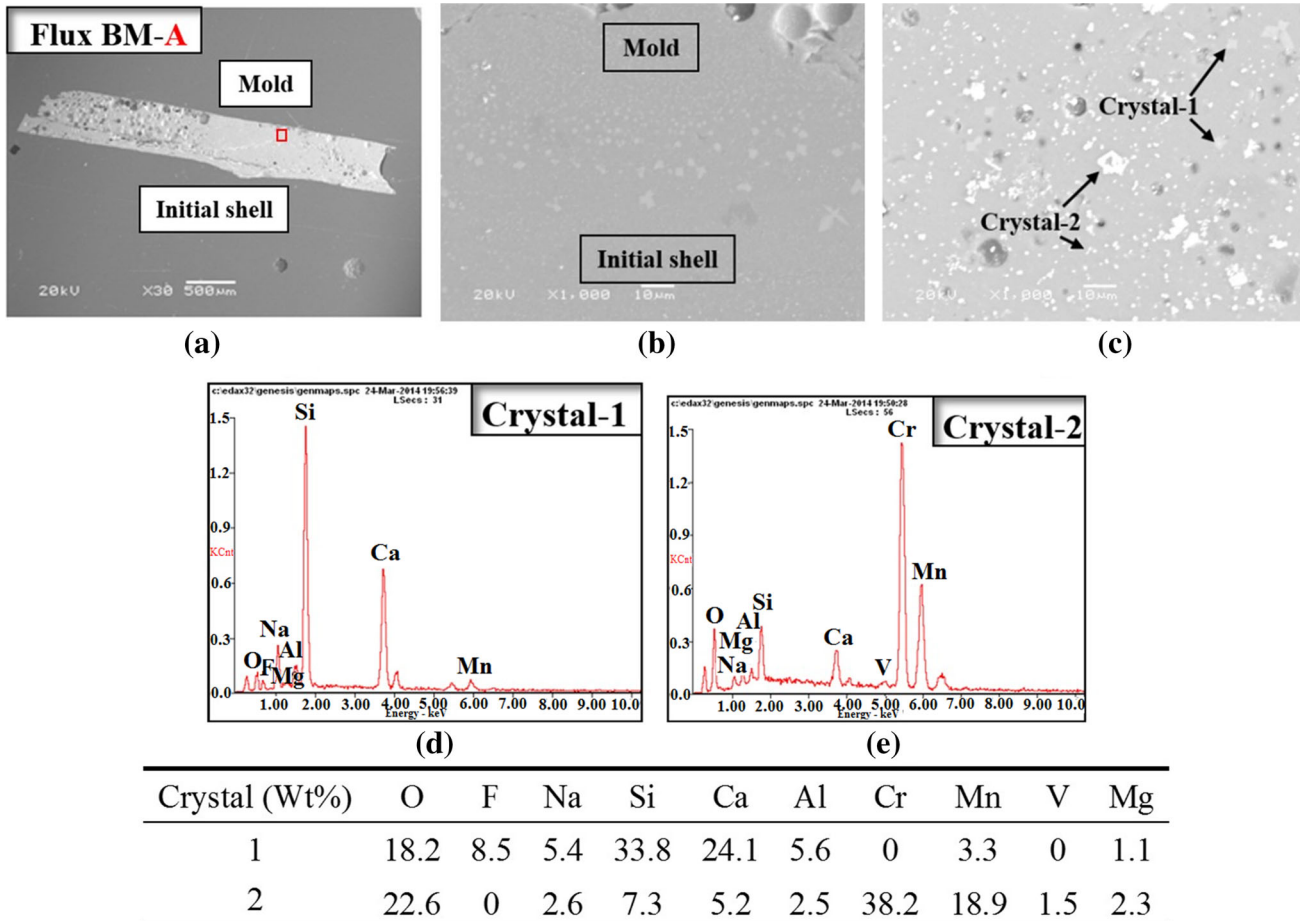


Fig. 5—SEM photos and EDS results of Flux BM at position A. (a) The overview of slag film at position A, (b) the amplified part of the zoom in (a), (c) two typical morphologies of crystalline phases in Flux BM, (d) and (e) the energy spectra of EDS for both crystals.

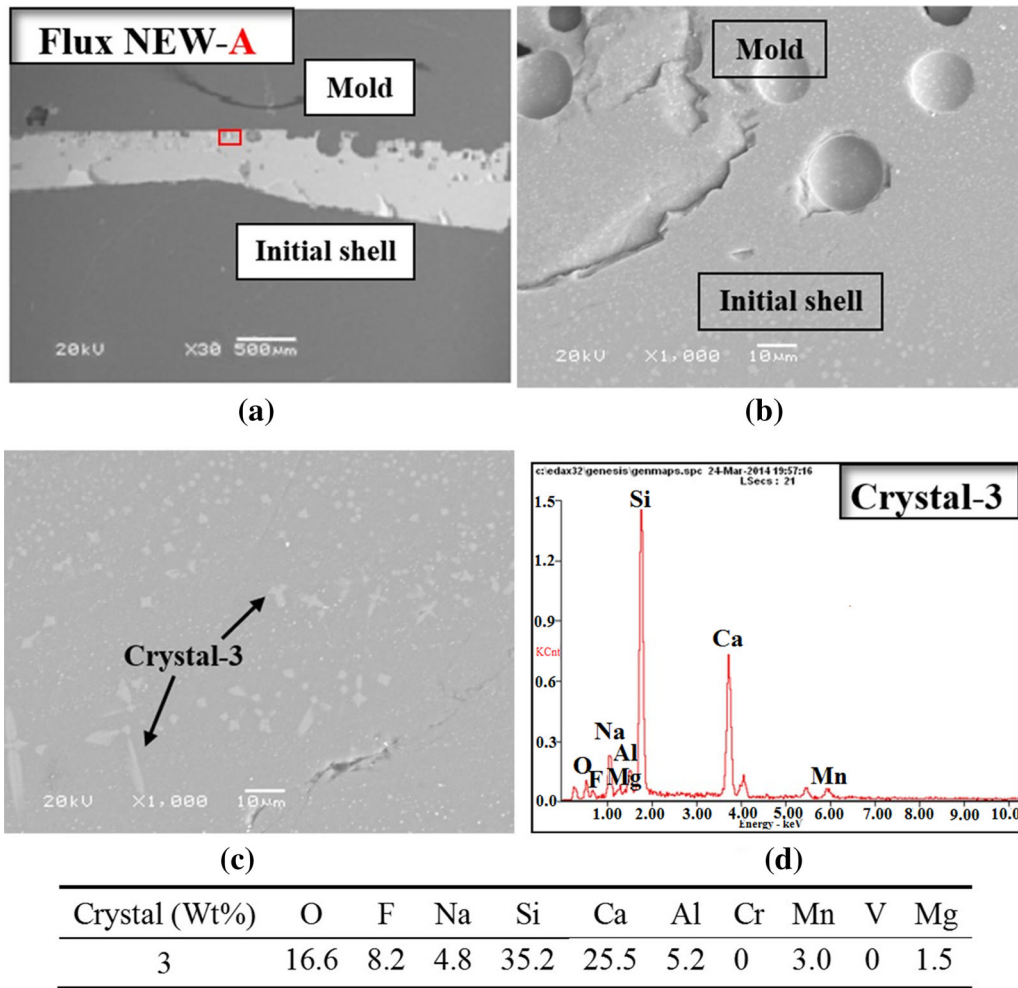


Fig. 6—SEM photos and EDS results of Flux NEW at position A. (a) The overview of slag film at position A, (b) the amplified zoom in the box part in (a), (c) typical morphology of crystalline phase in Flux NEW, (d) the energy spectra of EDS for crystal-3.

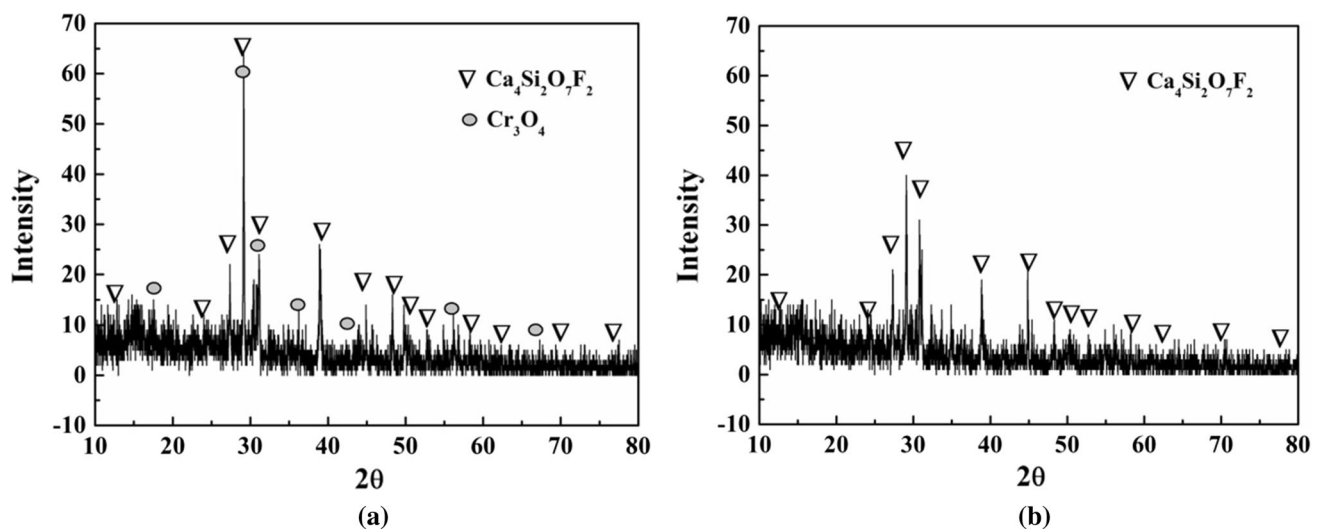


Fig. 7—XRD patterns of mold fluxes for (a) Flux BM and (b) Flux NEW.

mold fluxes are used, as shown in Figure 8. First, it can be seen intuitively that the amplitude of the temperature fluctuations for Flux BM is larger than that of Flux

NEW, especially in the casting period stage III. Second, even though the initial temperatures at the beginning of the casting period for both cases are pretty close, the

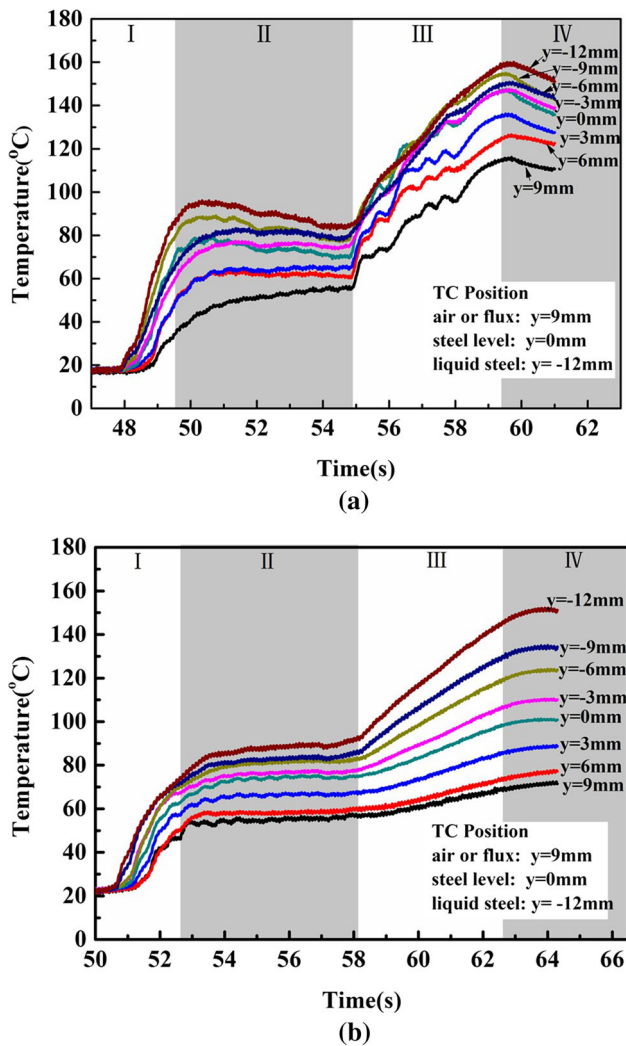


Fig. 8—Calculated hot surface temperature profile during the simulation casting experiment for the cases of (a) Flux BM and (b) Flux NEW.

responding temperature of the mold hot face in the case of Flux BM is relatively higher during the casting period compared with the case of the Flux NEW system (in stage III). The maximum temperature in Figure 8(a) is 433 K (160 °C), while the maximum temperature in Figure 8(b) is 424 K (151 °C). Third, in the casting period stage III, temperature distribution in the case of Flux NEW is more uniform. The main reason for the preceding phenomena is directly related to the infiltration of the liquid mold flux in the gap between the initial shell and the mold hot face. In the case of the Flux BM casting experiment, the contact between the mold and the initial solidified shell is not perfect due to the formation of the discontinuous slag film, which in turn leads to the significant variation of the responding temperature, as shown in Figure 8(a). In the case of Flux New, the well-formed relatively thick mold-flux film would insulate and homogenize the heat transfer in the mold; thus, a uniform and low-temperature gradient in the mold would result, as in Figure 8(b).

Figure 9 shows the evolution of heat flux across the mold hot face around the melt level ($y = -3, 0, \text{ or } 3$ mm) during the casting period, where Figures 9(a) and (b) show the heat-flux distribution for the case of Flux BM and Flux NEW, respectively. It can be found from Figure 9 that the heat flux oscillated periodically with a frequency of 1.7 Hz, almost the same as the mold oscillation through the preliminary observation and estimation, which indicates that the fluctuation of heat flux mainly results from mold oscillation. It also can be observed that the magnitude of oscillation for the heat flux at the melt level ($y = 0$ mm) is larger than others, *i.e.*, the positions below ($y = -3$ mm) and above ($y = 3$ mm) the melt level, as the mold direct oscillated in and out of the molten steel pool.

Besides, the baseline of the fluctuant heat-flux curve at the melt level ($y = 0$ mm) in Figure 9(a) is about 2.0 Mw/m^2 with a stroke of about 0.3 Mw/m^2 , while at the same position in Figure 9(b), the baseline is 1.25 Mw/m^2 with a stroke of 0.1 Mw/m^2 . This suggests that both the heat flux and the fluctuation of the heat flux during the casting process with Flux BM are larger than those of the Flux NEW case. With the accumulation of chromium and manganese oxide inclusions, the infiltration of Flux BM became even worse, such that the entire slag film could not be formed between the initial shell and the mold during the process of casting, as shown in Figures 2 and 3(a). Therefore, the insufficient infiltration of mold flux would force the molten steel, or the initial solidified shell directly touches the hot face of the mold during the casting process. An interesting phenomenon can be found in Figure 2, that when the surface of the shell is convex, no slag film exists, such as the top right part of the shell. However, for the position with slag film, the surface is concave, such as the top left part of the shell. So, the insufficient slag film between the mold hot face and the initial solidified shell would introduce a varied and lower thermal resistance from the molten bath to the mold wall, which would result in a higher and more varied heat flux during the casting process with Flux BM.

C. Surface Profile of Initial Shells with Different Mold Flux

The initial solidified shells after casting experiments were cut off and are shown in Figure 10, among which Figure 10(a) is the shell profile for the case of Flux BM and Figure 10(b) is for the case of Flux NEW. The shell is constituted of two zones: the major top one is the casting stage zone, which corresponds to casting stage III in Figure 8, and the bottom one is the holding stage zone, which corresponds to holding stage II in Figure 8. The length of the casting shell is about 54 mm, which is equal to the product of casting speed (12 mm/s) by casting time (4.5 seconds).

It can be seen from Figure 10(a) that the surface of the shell obtained from the case of Flux BM is quite uneven, with many severe depressions, cracks, and wrapped slags. Those typical defects were mainly caused by the lack of lubrication during the casting process. However, the surface quality of the shell obtained in the

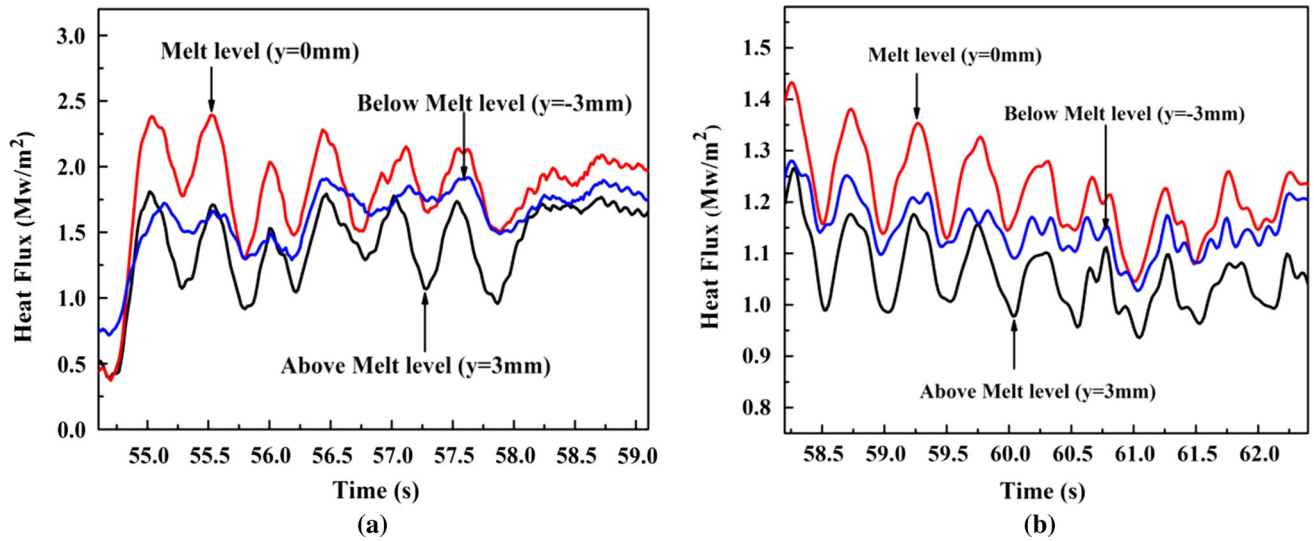


Fig. 9—Heat fluxes around the meniscus during the casting simulation experiments for the cases of (a) Flux BM and (b) Flux NEW.

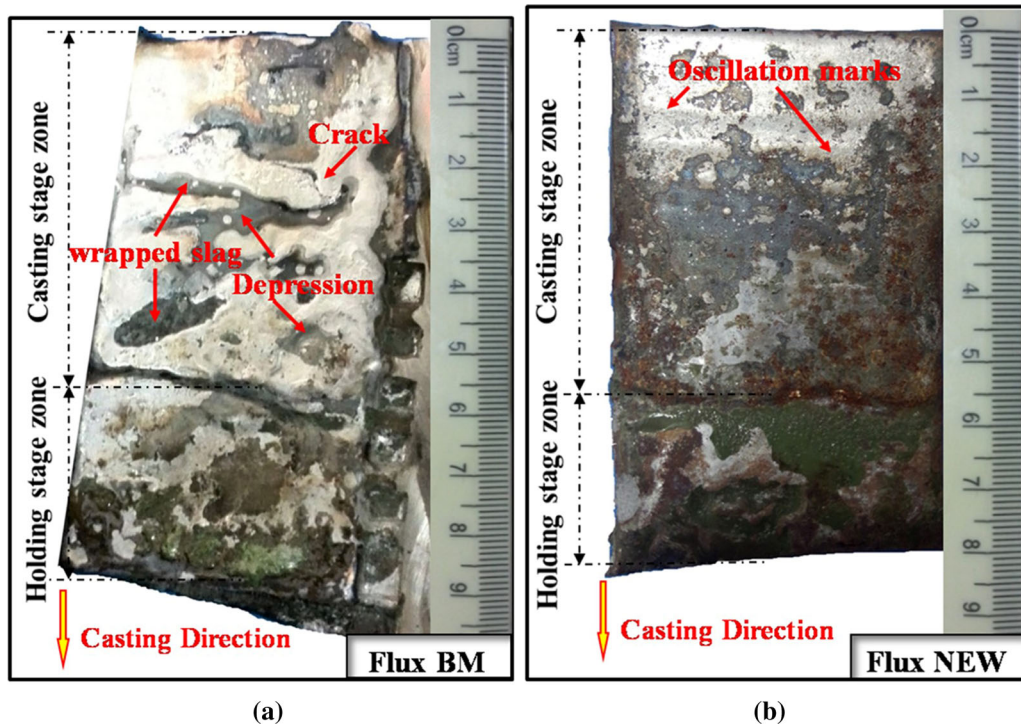


Fig. 10—Surface profiles of initial shells for the cases of (a) Flux BM and (b) Flux NEW.

Flux NEW case is much smoother, as shown in Figure 10(b). Besides, the shallow oscillation marks can also be found on the surface of the shell in Figure 10(b). Therefore, through combining the analysis results of the preceding figures, it can be concluded that the appropriate infiltration of the molten slag and an even slag film distribution are the prerequisites for the effective control of the horizontal heat transfer during the initial solidification of molten steel in the mold; thereby, a better surface quality of the solidified slab could be obtained during the continuous casting process.

IV. CONCLUSIONS

The performance of mold fluxes for the casting of Cr12MoV alloy steel was investigated by the application of a mold simulator in this study. The structure of slag film, responding temperature, and heat flux across the mold hot face and surface profile of the initial shell were studied. The major conclusions are summarized as follows.

1. The slag film formed in the case of Flux BM is thin and discontinuous, due to the absorption of Cr_3O_4 inclusions from the molten steel into the liquid mold

slag, while the slag film formed in the case of the optimized Flux NEW is uniform due to the addition of B_2O_3 , which could compensate for the influence caused by the pickup of chromic oxide in the mold flux. Circular holes were found in the slag film close to the mold side, as the holes formed in the mold flux close to the mold side could not be refilled, due to the lack of fluidity of the mold flux in the low-temperature zone.

2. The main precipitated crystals in Flux BM were cuspidine ($Ca_4Si_2O_7F_2$) and Cr_3O_4 , while only $Ca_4Si_2O_7F_2$ precipitated in Flux NEW. The thicknesses of the slag film, at the top and middle parts, were 0.51 and 0.68 mm for Flux BM, while they were 0.62 and 0.85 mm for Flux NEW.
3. Both the responding temperature and heat flux across the mold hot face in the case of Flux BM were relatively higher and fluctuated more dramatically than those in the case of Flux NEW tests, as the insufficient infiltration of the mold flux would result in a varied and lower thermal resistance during the casting experiment with Flux BM.
4. The surface of the shell obtained in the Flux BM casting experiment is quite uneven, with many severe depressions, cracks, and wrapped slag because of the insufficient lubrication during the casting process. However, the surface quality of the shell obtained in the Flux NEW case is smooth.

ACKNOWLEDGMENT

The final support from Newton Advanced Fellowship (Grant No. NA 150320) and NSFC (Grant Nos. 51504294 and 51661130154) is gratefully acknowledged.

REFERENCES

1. K.C. Mills, A.B. Fox, Z. Li, and R.P. Thackray: *Ironmak. Steelmak.*, 2005, vol. 32 (1), pp. 26–34.
2. W. Wang, L. Zhou, and G. Kezhuan: *Met. Mater. Int.*, 2010, vol. 16 (6), pp. 913–20.
3. C. Li and B.G. Thomas: *Metall. Mater. Trans. B*, 2004, vol. 35B, pp. 1151–72.
4. S. Sridhar, K.C. Mills, and S.T. Mallaband: *Ironmak. Steelmak.*, 2002, vol. 29 (3), pp. 194–98.
5. G. Kim and I.L. Sohn: *ISIJ Int.*, 2012, vol. 52 (1), pp. 68–73.
6. R.M. McDavid and B.G. Thomas: *Metall. Mater. Trans. B*, 1996, vol. 27B, pp. 672–85.
7. L. Zhou, W. Wang, R. Liu, and B.G. Thomas: *Metall. Mater. Trans. B*, 2013, vol. 44B, pp. 1264–79.
8. M. Valdez, G.S. Shannon, and S. Sridhar: *ISIJ Int.*, 2006, vol. 46 (3), pp. 450–57.
9. C. Shi, M. Seo, J. Cho, and S. Kim: *Metall. Mater. Trans. B*, 2014, vol. 45B, pp. 1081–97.
10. H. Nakada and K. Nagata: *ISIJ Int.*, 2006, vol. 46 (3), pp. 441–49.
11. Y. Kashiwaya, C.E. Cicutti, A.W. Cramb, and K. Ishii: *ISIJ Int.*, 1998, vol. 38 (4), pp. 348–56.
12. L. Zhou, W. Wang, F. Ma, J. Li, J. Wei, H. Matsuura, and F. Tsukihashi: *Metall. Mater. Trans. B*, 2012, vol. 43B, pp. 354–62.
13. L. Zhou, W. Wang, D. Huang, J. Wei, and J. Li: *Metall. Mater. Trans. B*, 2012, vol. 43B, pp. 925–36.
14. H.G. Ryu, Z.T. Zhang, J.W. Cho, G.H. Wen, and S. Sridhar: *ISIJ Int.*, 2010, vol. 50 (8), pp. 1142–50.
15. H. Mizuno, H. Esaka, K. Shinozuka, and M. Tamura: *ISIJ Int.*, 2008, vol. 48 (3), pp. 277–85.
16. M. Susa, A. Kushimoto, H. Toyota, M. Hayashi, R. Endo, and Y. Kobayashi: *ISIJ Int.*, 2009, vol. 49 (11), pp. 1722–29.
17. J. Diao, B. Xie, and J.P. Xiao: *Ironmak. Steelmak.*, 2009, vol. 36 (8), pp. 610–64.
18. L. Zhou, W. Wang, J. Wei, and M. Jin: *ISIJ Int.*, 2013, vol. 53 (4), pp. 665–72.
19. L. Zhou, W. Wang, J. Wei, and K. Zhou: *ISIJ Int.*, 2015, vol. 55 (4), pp. 821–29.
20. G. Wen, S. Sridhar, P. Tang, X. Qi, and Y. Liu: *ISIJ Int.*, 2007, vol. 47 (8), pp. 1117–25.
21. M. Hayashi, R.A. Abas, and S. Seetharaman: *ISIJ Int.*, 2004, vol. 44 (4), pp. 691–97.
22. A. Yamauchi, K. Sorimachi, T. Sakuraya, and T. Fujii: *ISIJ Int.*, 1993, vol. 33 (1), pp. 140–47.
23. D.T. Stone and B.G. Thomas: *Can. Metall. Q.*, 1999, vol. 38 (5), pp. 363–75.
24. L. Zhou, W. Wang, B. Lu, G. Wen, and J. Yang: *Met. Mater. Int.*, 2015, vol. 21 (1), pp. 126–33.
25. E. Wei, Y. Yang, C. Feng, I.D. Sommerville, and A. Mclean: *J. Iron Steel Res. Int.*, 2006, vol. 13 (2), pp. 22–26.
26. A.W. Cramb: *AISI/DOE Technology Roadmap Program*, American Iron and Steel Institute, Pittsburgh, PA, 2003.
27. E. Jung, W. Kim, I. Sohn, and D. Min: *J. Mater. Sci.*, 2010, vol. 45 (8), pp. 2023–29.
28. M. Hanao and M. Kawamoto: *ISIJ Int.*, 2008, vol. 48 (2), pp. 180–85.
29. P.O. Hooli: *Ironmak. Steelmak.*, 2002, vol. 29 (4), pp. 293–96.
30. A. Badri, T.T. Natarajan, C.C. Snyder, K.D. Powers, F.J. Mannion, M. Byrne, and A.W. Cramb: *Metall. Mater. Trans. B*, 2005, vol. 36B, pp. 373–83.
31. E. Ko, J. Choi, J. Park, and I. Sohn: *Met. Mater. Int.*, 2014, vol. 20 (1), pp. 141–51.
32. H. Zhang, W. Wang, F. Ma, and L. Zhou: *Metall. Mater. Trans. B*, 2015, vol. 46B, pp. 2361–73.
33. H. Zhang and W. Wang: *Metall. Mater. Trans. B*, 2016, vol. 47B, pp. 920–31.
34. H. Zhang, W. Wang, D. Zhou, F. Ma, and L. Zhou: *Metall. Mater. Trans. B*, 2014, vol. 45B, pp. 1038–47.
35. H. Zhang, W. Wang, and L. Zhou: *Metall. Mater. Trans. B*, 2015, vol. 46B, pp. 2137–52.
36. C. Xu, W. Wang, L. Zhou, S. Xie, and C. Zhang: *Metall. Mater. Trans. B*, 2015, vol. 46B, pp. 882–92.
37. K. Mills: *ISIJ Int.*, 2016, vol. 56 (1), pp. 14–23.
38. K. Mills, S. Karagadde, P. Lee, L. Yuan, and F. Shahbazian: *ISIJ Int.*, 2016, vol. 56 (2), pp. 264–73.